Pergamon

PII: S0301-9322(96)00012-2

Int. J. Multiphase Flow Vol. 22, No. 4, pp. 733–751, 1996

0301-9322/96 $15.00 + 0.00

A COMPUTER BASED HOT-FILM TECHNIQUE USED FOR FLOW MEASUREMENTS IN A VERTICAL KEROSENE–WATER PIPE FLOW

B. FARRAR and H. H. BRUUN

Department of Mechanical and Manufacturing Engineering, Bradford University, Bradford BD7 1DP, U.K.

(Received 27 January 1993; in revised form 7 February 1996)

Abstract—This paper presents the application of a hot-film anemometer based two-phase flow measurement technique to the investigation of the structure of a vertical pipe flow of a water–kerosene mixture. Experiments were carried out within the bubbly flow, spherical cap bubble and churn flow regimes. The results obtained show that the radial profile of the local volume fraction is uniform at low volumetric quality, β, but becomes wall peaked as β increases. The average oil drop size is uniform across the pipe and independent of β for values of β below 15%, but at higher values the drop size increases in the central region of the pipe. The velocity profile becomes more uniform as β increases from zero to about 15%, but then becomes steeper again at higher values of β, and the variation of the centreline turbulence intensity with β shows a local minimum for $\beta \cong 20\%$. The one-dimensional energy spectrum for the water–kerosene mixture flow is found to be composed of two power laws with exponents -1 at lower frequencies and $-5/3$ at higher frequencies, and the characteristic length scales associated with the continuous phase turbulence decrease substantially with increasing β. Copyright © 1996 Elsevier Science Ltd.

Key Words: multi-phase flow, oil–water flow, hot-film anemometry

1. INTRODUCTION

Turbulent bubbly two-phase flow occurs in many industrial environments, such as nuclear reactors, oil extraction bore wells and petro-chemical plants.

With the advent of CFD (Computational Fluid Dynamic) computer models a predictive need has developed for more accurate and detailed simulations of two-phase flows. Modelling of bubbly two-phase flow require the specification of interfacial and wall transfer laws as well as a reasonably accurate description of the interaction between the bubbles and the continuous phase. To develop such models it is necessary to obtain a physical understanding of the mechanisms involved in the local transfer processes, which takes place in turbulent two-phase flows. Although there are numerous papers on pressure drop, wall stresses and profiles of void fraction and phase velocities in pipe flows, there is still only relatively few papers dealing with the measurements or prediction of the turbulent structure of gas/liquid two-phase flows. The pioneering works of Serizawa *et al.* (1975) and Herring & Davis (1976) used a resistivity probe to measure void fraction, bubble size as well as parameters which would be used to characterise the developing two-phase flow structure. In particular two techniques have been used to study the local turbulent structure of the continuous phase, namely Laser Doppler Anemometry (LDA) and Hot-Film Anemometry (HFA). LDA has the advantage of being non-intrusive, but it requires a clear optical path and reported measurements are in general restricted to low void fractions ($\epsilon < 5\%$). In contrast HFA can in principle be applied to flows with either low or high void fraction.

Turbulence measurements in gas/liquid flows have predominantly been reported for vertical up or down flows in circular pipes (Serizawa *et al.* 1975; Sato & Sekoguchi 1975; Sullivan *et al.* 1978; Theofanous & Sullivan 1982; Michiyoshi & Serizawa 1986; Wang *et al.* 1987; Souhar 1989; and Liu & Bankoff 1993). Additional two-phase flow turbulence measurements has been carried out in a narrow channel by Jones & Zuber (1978) and in a large square vertical channel flow for the cases of uniform grid turbulence (Lance & Bataille 1991) and in the boundary layer on a flat plate (Moursali *et al.* 1995). These investigations have demonstrated that the flow structure and the

profile distributions can be greatly dependent on: (i) the initial bubble generation and mixing conditions, (ii) the flow rates and physical properties of the two phases and (iii) the geometry and wall conditions of the test section.

Regarding the lateral redistribution of the two phases, the importance of bubble size and geometry in the lateral migration of bubbles have been studied and discussed as a key parameter in flow modelling in a number of recent papers (Serizawa & Kataoka 1987; Zun 1988; Kataoka 1992; and Tomiyama *et al.* 1995).

The study of "bubbly" flow of two immiscible liquids can provide valuable insight into the parameter dependence of the turbulence in the continuous phase, as the "bubble"/continuous phase interaction and structure development will be different from that of a gas/liquid flow. There is currently no published data available on the turbulent structure of the flow of two immiscible liquids in a vertical pipe. This paper presents the first set of data from a study of oil/water up-flow in a vertical pipe. Where ever practical the data presented in this paper has been compared with related results for gas/liquid flows as well as being discussed within the context of current proposed mechanisms for lateral bubble migrations.

2. THE TWO-PHASE KEROSENE–WATER FLOW LOOP

The test facility was designed to deliver a mixture of water and kerosene of known, variable composition to the chosen test section. Therefore, the flow rates of the two fluids were measured separately before being mixed upstream of the test section. The vertical test section was placed in a recirculating test rig and one cannot be sure that the mixture returning to the storage tank will have sufficient time to separate naturally without the use of an exceedingly large container. A device is therefore required to enhance separation to ensure that no dispersion enters the storage reservoir, as described in section 2.1.

The design of the flow loop test facility is shown in figure 1, with the key components identified as numbers 1–10. Briefly the test facility comprises: a combined storage tank/separator (1) for the water and kerosene. From the bottom of the separate reservoirs of kerosene and water in the storage tank fluid is delivered by two pumps (2) to two horizontal pipes containing the flow metering equipment. At the entrance to each pipe is installed a swirl remover and flow conditioner unit (3) in order to achieve "fully developed" turbulent flow at the position of the flow meters (4). (Details are given in Farrar and Bruun 1988.) The two metered fluids are then mixed in a Y junction

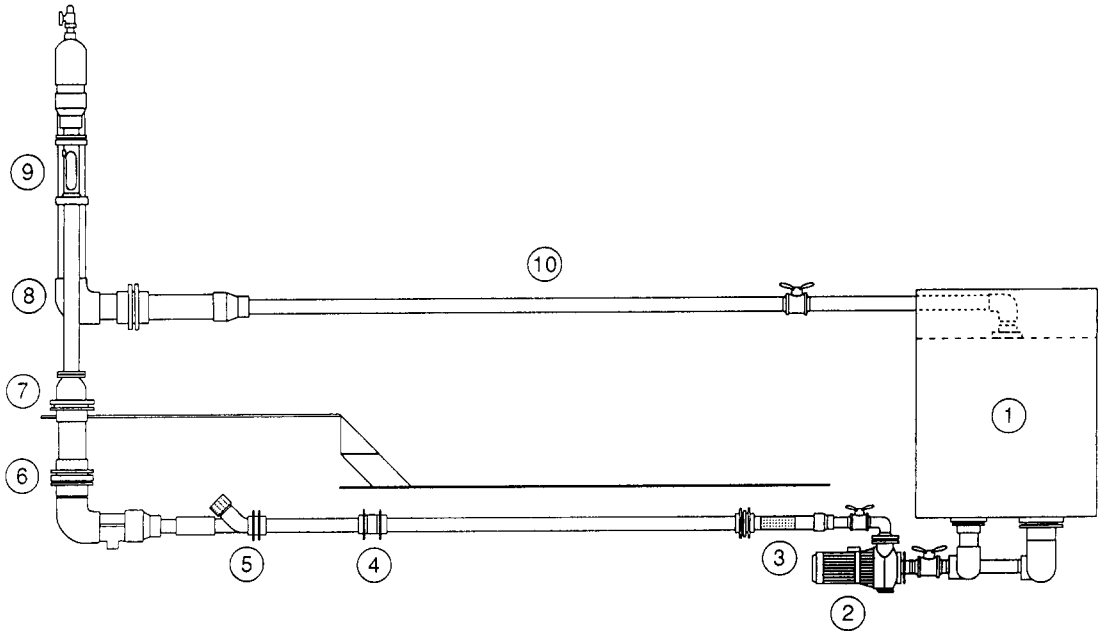

Figure 1. Water–kerosene flow loop test facility.

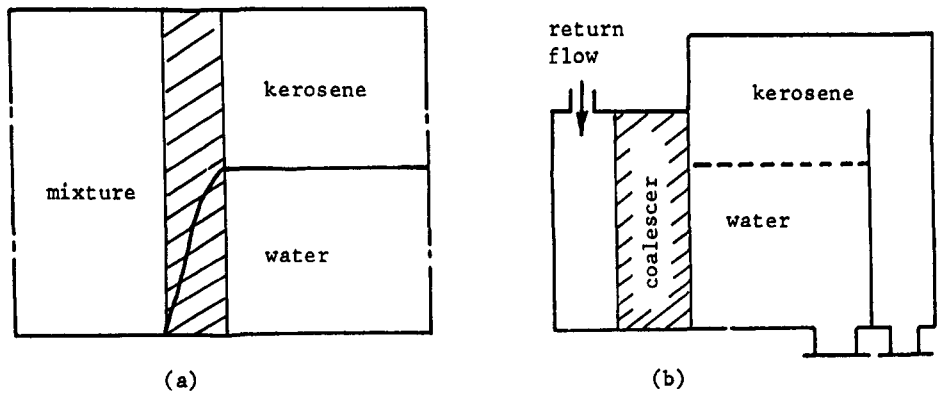

Figure 2. (a) Principle of knitmesh coalescer; (b) Storage tank/separator.

(5), followed by a 90° bend to provide the required vertical flow. A swirl remover and flow conditioning unit is positioned at (6) followed by a contraction unit (7). The purpose of these units is to produce as near as possible fully developed two-phase flow at the end of the test section. The test section, described in section 2.2, consists of a development length (8) and a measurement section (9) used for detailed hot-film anemometer studies. The return loop contains a horizontal part (10) of significant length, which may be used for future horizontal pipe flow studies.

2.1. Separation and storage of component fluids

The levels of solubility of water in kerosene and vice versa are so low that, for all practical purposes, the two fluids may be regarded as being totally immiscible, and when they are mixed together they will form a dispersion, in which drops of one of the fluids are dispersed in the other fluid. The type of dispersion, i.e. kerosene drops in water or vice versa, depends on the relative volumes of the two fluids and on the method of mixing. If a water–kerosene dispersion is allowed to stand for a sufficient length of time then it will settle out naturally due to the difference in density between the two fluids. However, in a recirculating test rig it is unlikely that the mixture returning to the storage tank will have sufficient time to separate naturally. The construction of a special separator was therefore required.

Since the test facility must be capable of creating flowing mixtures ranging from 100% water to 100% kerosene then phase inversion (i.e. the dispersed phase becomes the continuous phase and vice versa) will take place at some stage and a coalescer is required that can cope with both water in kerosene dispersions and kerosene in water dispersions. The authors came across only one type which could cope with such demanding conditions. This is the Knitmesh DC coalescer which consists of a mesh screen, 300 mm thick, made up of a fabric knitted with a combination of metal wire and plastic filaments. The metal has a high surface free energy whereas the plastic has a low surface free energy. It has been found (Knitmesh 1982) that the coalescence of droplets is greatly enhanced at a point at which there is a discontinuity of surface free energy, e.g. where a plastic filament crosses a metal wire. This type of coalescer is therefore more efficient than the conventional packing materials which require that the dispersed phase preferentially wets the material. However, the most important advantage of the Knitmesh coalescer is that it can operate through phase inversion with no loss of efficiency. Figure 2(a) shows the operation of the coalescer in cross flow. Provided the equipment is sized correctly, then no dispersion will be present on the downstream side of the coalescer.

The dimensions of the coalescer dictate the size of the storage vessel since the two may be combined. The design selected is shown in figure 2(b). The flowing mixture returns to the vessel and enters a settling chamber. From here it passes through the coalescer element where the water and kerosene are separated. The kerosene flows over a baffle plate and into its own separate storage area. The water and kerosene outlets are on the underside of the tank.

2.2. Test section

The test section of the flow loop is a 1.5 m vertical length of 78 mm diameter circular tube. It is transparent to allow flow visualisation and has the facility to insert a hot-film probe near the downstream end. The tube material was cast acrylic tubing due to its good optical and mechanical properties. As stated earlier, mixing was achieved by bringing the two pipelines together using a Y junction. The mixture then flowed through a 6″ diameter 90° elbow and into the vertical section via a smooth contraction unit. The combination of the elbow and the mixing of the two fluids produces a disturbed swirling flow. To remove the existing swirl a tube bundle consisting of four tubes was constructed and fitted just upstream of the contraction unit. This appeared to cure the swirl problem, but left a slightly distorted velocity profile at the inlet to the test section.

The development of mean velocity and volume fraction profiles has been reported in several investigations. Serizawa *et al.* (1975) found that in their air-water two-phase flow loop, using a sharp edged intake, both profiles were highly non-symmetrical at a position ten diameters (10 D) from the entrance. At 20 D the profiles were approaching axial symmetry but still changing slightly and at 30 D the axial symmetry was very good. The authors concluded that nearly fully developed flow was attained at 30 D from the entrance for bubbly flows and that for slug flows the development length was even shorter. However, the development length is very much dependent upon the entrance conditions and upon the way in which the fluids are mixed. Herringe & Davis (1976) investigated the development of two-phase vertical gas–liquid flows using various mixing and entrance conditions. The authors measured void fraction profiles at 8, 36 and 108 diameters from the entrance. At 8 D the profiles were highly dependent upon the method of mixing, but at 108 D the profiles were almost independent of the mixing conditions. They observed that a nearly fully developed void fraction profile was obtained at 36 D when a perforated screen or grid and a smooth contraction were used after the mixing. In the current test rig there is, after the swirl remover unit and smooth contraction unit, 17 diameters of straight pipe before the hot-film instrumentation. This provided nearly fully developed flow conditions at the measurement position.

3. INSTRUMENTATION AND SIGNAL ANALYSIS PROCEDURE

The measurements were carried out using a single normal DANTEC 55R11 fibre probe, mounted in a DANTEC 55H540 watertight mounting tube, which has a 90° bend. This enabled the probe to be placed with the prongs parallel to the flow direction, thus facilitating the piercing of the drops in the kerosene–water flow mixture. The hot-film probe was operated by a DANTEC 56C anemometer at an overheat ratio of 1.05 to avoid formation of air bubbles on the hot-film element. The output from the anemometer was fed to a signal conditioning unit with offset and gain. The purpose of this unit was to match the hot-film signal to the full range (0–10 V) of the 12 bit analogue to digital converter A/D used. The data acquisition and analysis system was based on a micro-computer, using a sampling rate of 1667 Hz and a total measuring time of 9.83 s.

The digital technique used for discrimination between the oil drops and the continuous water phase and the signal analysis procedure for the continuous phase signal part is described in Farrar (1988), Bruun (1995), Bruun & Samways (1995), Bruun *et al.* (1995) and Farrar *et al.* (1995).

In order to obtain reliable results when using hot-film anemometry it is important that the probe is accurately calibrated. This was performed *in situ*, i.e. in the test section of the flow loop, in single-phase water flow, using the calibration relationship,

$$E^2 = A + BU^n \qquad [1]$$

as described in Farrar (1988). An improved computer based calibration technique is described by Samways *et al.* (1994).

As explained by e.g. Bruun (1995) the application of hot-film probes in water can be severely affected by drift of the calibration due to the accumulation of dirt on the surface of the sensor. To reduce this problem a relatively coarse by-pass filter was fitted to the water storage tank. However, the filter used did not completely eliminate the water contamination problem. As a consequence fairly frequent probe calibrations were necessary.

4. INITIAL MEASUREMENTS

The hot-film probe was arranged so that the axis of the cylindrical sensor was perpendicular to the radial direction (i.e. tangentially oriented) and it was traversed radially over a range of 0–36 mm (pipe radius 39 mm). To establish whether the flow was axi-symmetric, the complete test section, including probe, could be rotated. Initial measurements were carried out both for single phase (water) and water–kerosene mixture flow in the following referred to as two-phase flow by placing the probe for each radial position at four angular positions, 0, 90, 180 and 270°. For the single phase measurements, a Reynolds number Re_D of 50,000 was chosen for compatibility with measurements of Laufer (1954) and Resch (1970). The measured mean velocity ($\bar{U}/\bar{U}_c$) and turbulence intensity ($u'/\bar{U}_c$) profiles were found to be close to those reported by Laufer (1954). ($\bar{U}$ = local mean velocity, $\bar{U}_c$ = centreline mean velocity and $u' = (\overline{u^2})^{1/2}$.) A close examination showed that the mean velocity profile was slightly skewed, due to the non-uniformities at the inlet to the vertical pipe section (Farrar 1988). However, the presence of drops in the two-phase flow studies reduced the axial development length considerably, and the initial measurements showed that the two-phase flow was axi-symmetric at the test position. The majority of the results presented were therefore obtained from a traverse along one radius only at an axial position X/D of 17.

5. TWO-PHASE FLOW MEASUREMENTS

The single-phase flow development tests were carried out at a flow rate of 185 l/min, giving a Reynolds number of 50,000, so that a direct comparison could be made with the data of Laufer (1954) and Resch (1970). For the two-phase flow tests the total mixture flow rate was arranged to be the same for all tests and equal to that of the single-phase flow tests, i.e. 185 l/min. The majority of the tests were performed over a range of values of the volumetric quality β from 5 to 30% at 5% intervals. Due to the normal reference to a bubbly flow regime and for ease of comparison with liquid–gas two-phase flow, we will in the following refer to the oil drops as "bubbles". The above mentioned flow conditions covered the bubbly flow regime and span the range from the flow of distributed, non-interacting bubbles to the flow of packed, interacting bubbles.

At all values of the volumetric quality β measurements were made of the radial profiles of the local volume fraction, mean bubble cord length, mean continuous phase velocity and turbulence intensity. In addition to these, centreline measurements were made of the pdf, autocorrelation function and Taylor's one-dimensional energy spectrum. The system was also applied, in a more limited way, to other types of flow, namely spherical cap bubble flow, churn flow and droplet (water dispersed) flow.

5.1. Bubbly flow, radial profiles

The measured radial profiles for the local volume fraction $\epsilon(r)$, mean bubble cord length $c(r)$, mean continuous phase velocity $\bar{U}/\bar{U}_c$ and turbulence intensity $u'/\bar{U}_c$ are shown in figures 3–6, respectively. At the lowest investigated volumetric quality, $\beta = 5\%$, the volume fraction profile $\epsilon(r)$, figure 3, shows a slight increase with radius but does not display the prominent wall peak seen in air–water flows at similar area averaged volume fraction (Sato & Sekoguchi 1975; Herringe & Davis 1976). This is probably due to the reduced buoyancy of the kerosene bubbles in comparison to air bubbles.

A number of studies have considered the origin, magnitude and direction of transverse forces acting on the dispersed flow. The interaction between the bubbles of the dispersed phase and the turbulent eddies of equivalent size appears to be a dominant mechanism (Serizawa & Kataoka 1992). This mechanism has been interpreted by, e.g. Sato & Sekoguchi (1975) and Beyerlein *et al.* (1985) in terms of a turbulent gradient transport term, while Serizawa & Kataoka (1987, 1992) and Tomiyama *et al.* (1995) has considered the lateral lift force caused by the asymmetric velocity field and complex vortex structure formed behind a distorted bubble. A number of researchers has also considered the lateral lift force on a bubble in a mean shear field caused by the liquid circulation around the bubble (Zun *et al.* 1975; Zun 1980; Beyerlein *et al.* 1985; Drew & Lahey 1987; Serizawa & Kataoka 1992; and Tomiyama *et al.* 1995). There is still some uncertainty as to the nature of

the lateral lift force acting on bubbles in a two-phase upwards flow, and for simplicity the model by Beyerlein *et al.* (1985) will be used for comparison between gas–liquid and liquid–liquid flows. They postulated a model for radial bubble distribution in two-phase systems in which they assumed that the mechanisms of distribution were two-fold. Firstly, there is a turbulent gradient transport term modelled as $j_{bt} = \epsilon_b \partial\epsilon/\partial r$ where j_{bt} is the volumetric bubble flux due to turbulent transport and ϵ_b is the bubble eddy diffusivity. Beyerlein *et al.* proposed that

$$\epsilon_b = K_b \epsilon_{mtp} \quad [2]$$

where K_b is a constant of order unity and ϵ_{mtp} is the two-phase eddy diffusivity introduced by Sato & Sekoguchi (1975), i.e.

$$\epsilon_{mtp} = (1 - \langle\epsilon\rangle)(\epsilon_{mL} + \langle\epsilon\rangle\epsilon_{mG}) \quad [3]$$

$$\epsilon_{mL} = K_L \frac{R}{6}\left[\frac{\gamma_w}{\rho_L}\right]^2\left[1 - \left[\frac{r}{R}\right]^2\right]\left[1 + 2\left[\frac{r}{R}\right]^2\right] \quad [4]$$

$$\epsilon_{mG} = K_G \langle\epsilon\rangle \frac{\langle d\rangle}{2} U_\infty \quad [5]$$

where $\langle\epsilon\rangle$ and $\langle d\rangle$ are the spatial mean values of the volume fraction and bubble diameter and U_∞ is the bubble free rise velocity (in quiescent water), K_L is the mixing length constant (≈ 0.4) and K_G an empirical constant. For similar values of the cross-sectional averaged volume fraction, the major differences in [2]–[5] between kerosene–water and air–water systems is in the values of $\langle d\rangle$ and U_∞. For kerosene–water $\langle d\rangle$ will probably be somewhat larger, but this will be

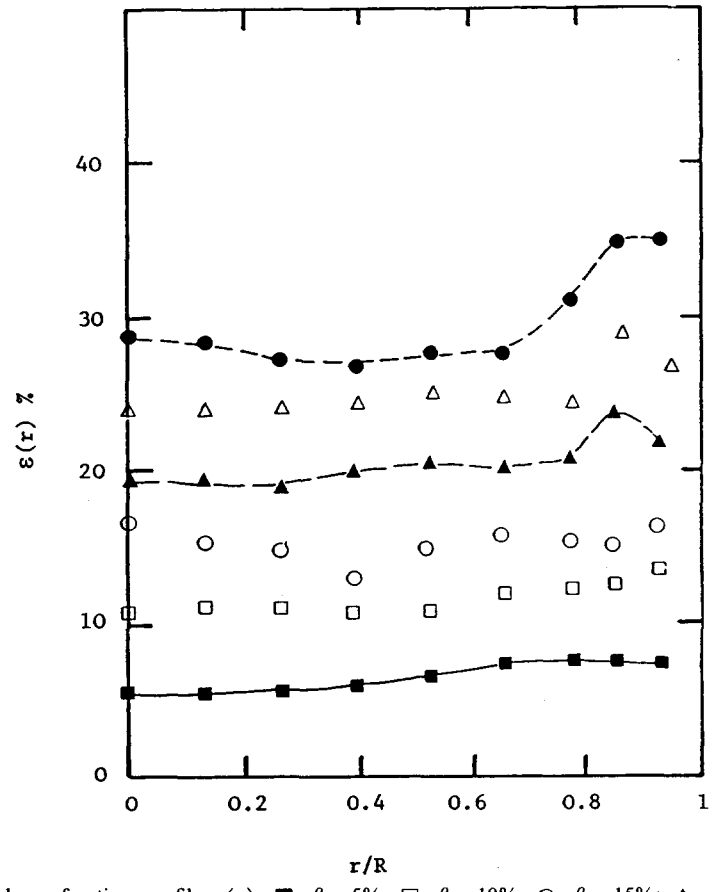

Figure 3. Volume fraction profile $\epsilon\langle r\rangle$; ■: $\beta = 5\%$; □: $\beta = 10\%$; ○: $\beta = 15\%$; ▲: $\beta = 20\%$, △: $\beta = 25\%$; ●: $\beta = 30\%$.

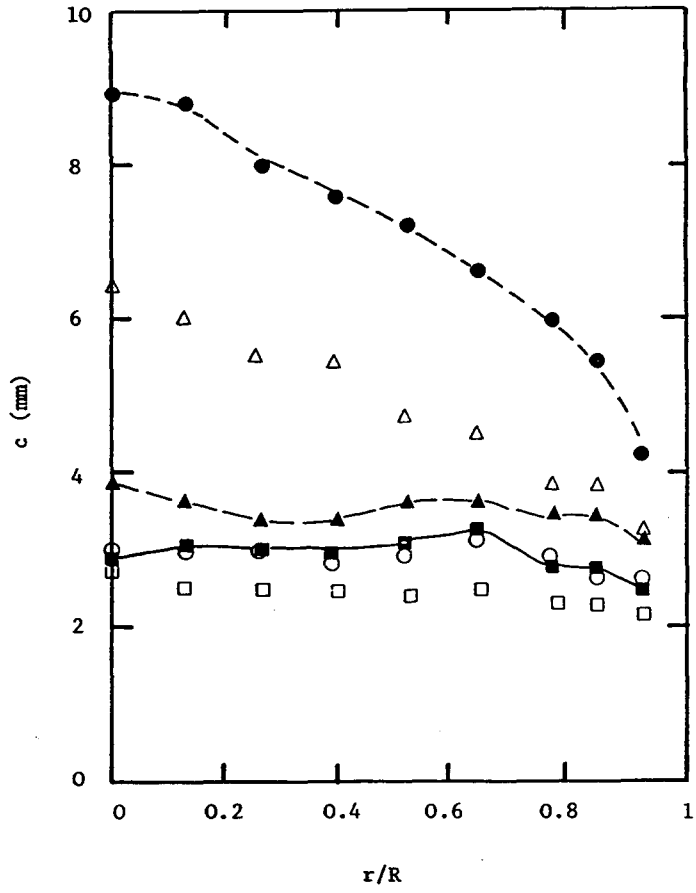

Figure 4. Bubble cut cord length $c(r)$ (see figure 3 for symbols).

counterbalanced by a lower value of U_∞. Consequently, the turbulent transport will be similar in both systems.

The second distribution mechanism is a result of a lateral force caused by the liquid velocity gradient acting on the bubbles (the net liquid circulation around the bubble). This force (per unit volume) is given by:

$$\mathbf{f}_m = C_1 \rho_L \mathbf{V}_{rel} \times \boldsymbol{\omega} \qquad [6]$$

where C_1 is a constant of order unity and ω is some angular velocity of the bubble, $\mathbf{V}_{rel}$ is the relative velocity of the bubble and $\times$ denotes the cross product of the two vector quantities. If the volume fraction is small, the relative velocity $\mathbf{V}_{rel}$ is equal to the rise velocity U_∞ of a small bubble in a quiescent container. The magnitude of ω can be approximated by

$$\omega \approx -C_2 \frac{\partial \bar{U}}{\partial r} \qquad [7]$$

where C_2 is another constant of order unity and $\bar{U}$ is the local mean continuous phase velocity. Beyerlein *et al.* also showed that the radial volumetric bubble flux due to the force $\mathbf{f}_m$ is given by

$$j_{bf} = -\frac{C_1 C_2}{g} \epsilon U_\infty^2 \frac{\partial \bar{U}}{\partial r}. \qquad [8]$$

The only difference in [8] between air–water and kerosene–water systems is the relative velocity of the bubbles. As the rise velocity of kerosene bubbles in infinite quiescent water is less than half that of air bubbles under similar conditions, the tendency for bubbles to migrate towards the tube wall is therefore much less in flows in which buoyancy forces are low.

Figure 4 shows the profiles of the mean bubble cut cord length obtained as described in Farrar (1988) and Bruun (1995). At $\beta = 5\%$ the distribution is seen to be fairly uniform across the pipe. The mean velocity profile for $\beta = 5\%$, figure 5, was found to be very similar to that measured in the single-phase flow ($\beta = 0\%$). However, comparing the turbulence intensity profile at $\beta = 5\%$ with the corresponding single-phase distribution, figure 6, reveals that the former is much more uniform and the centreline value is more than twice that of the single-phase flow.

The variation in the flow conditions with β can be identified from the results in figures 3–6. At $\beta = 10\%$ the volume fraction profile is almost identical in shape to that at $\beta = 5\%$ but with each value approximately twice the magnitude. The bubble cord length profile is again seen to be uniform. The velocity is very similar while the turbulence intensity has increased in magnitude.

At $\beta = 15\%$ the volume fraction profile is even more uniform. The bubble cut cord length shows little change but the mean velocity profile is observed to have become more uniform in the central region. The turbulence intensity is seen to have increased by a small amount over most of the cross-section.

Several developments take place when β is increased to 20%. The volume fraction profile is uniform over a large central portion but has a small peak close to the wall. This is in contrast to observations in air–water flows in which void profiles are wall peaked at low volumetric quality but become centre peaked as the volumetric quality increases. The formation of the peak close to the wall may be due to the change in the velocity profile which is now non-uniform over most of the cross section. Such a velocity profile may induce enhanced liquid circulation around the bubbles across a large part of the pipe area and, as [6] and [8] show a related increase in the lateral force exerted on the moving bubbles. There will therefore be a greater tendency for bubbles to migrate radially outwards (see [8] which involves $\partial \bar{U}/\partial r$). In addition to a general increase in the bubble cord length, c, from about 3 to 4 mm at the centreline, the profile of the bubble cord length now shows a slight decrease with increasing radius. This may be one reason for the more peaky mean

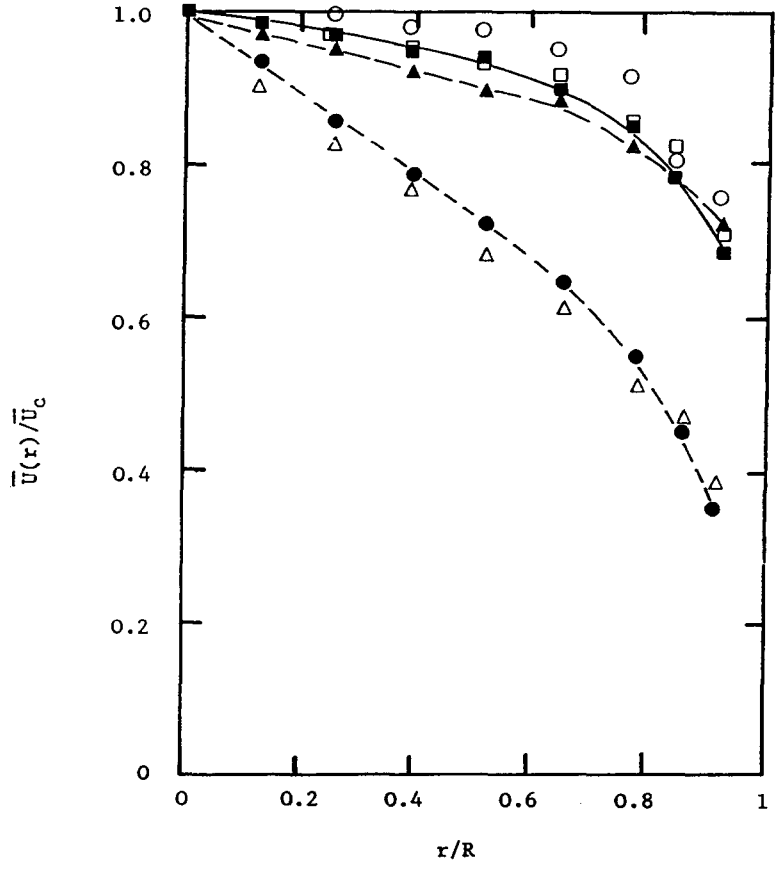

Figure 5. Normalised mean velocity profile $\bar{U}(r)/\bar{U}_c$ (see figure 3 for symbols).

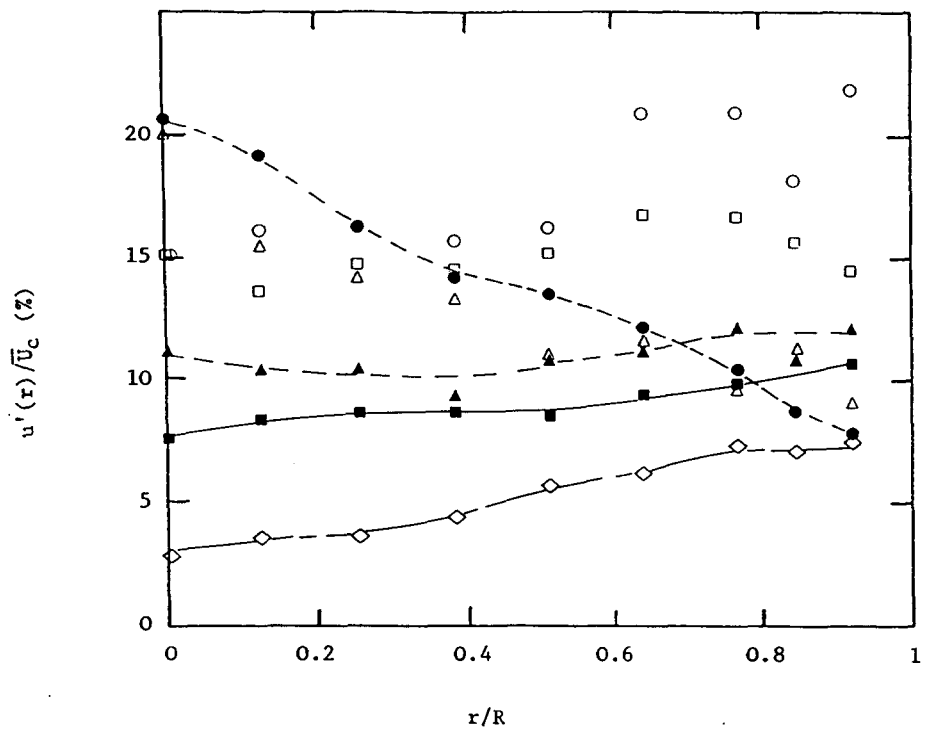

Figure 6. Turbulence intensity profile $u'(r)/\bar{U}_c$; ◇: $\beta = 0\%$; see figure 3 for other symbols.

velocity profile. Larger bubbles in the central region travel with a higher velocity and hence drive the continuous phase with greater speed. This results in a lower velocity in the outer regions of the pipe so that the overall continuous phase flow rate does not change. These changes are accompanied by a drop in the turbulence intensity over the complete cross-sectional area.

The above mentioned changes are even more pronounced when $\beta = 25\%$. The volume fraction profile has become clearly wall peaked, the mean bubble cord length profile is now very centre peaked and the mean velocity and turbulence intensity profiles are very steep over most of the cross-section. This trend continues for $\beta = 30\%$. There is now a relatively large peak in the volume fraction profile close to the wall and the average bubble cord length is about 9 mm on the centreline, indicating that the flow is approaching the spherical cap flow regime. These large bubbles travel much faster than the 4 mm diameter bubbles near the wall and are thus responsible for the highly centreline peaked velocity profile. Such a velocity profile will induce a substantial liquid circulation around the bubbles and is thus responsible for the migration of bubbles towards the pipe wall which results in the observed peak in the volume fraction profile. The changes in shape of the mean velocity profile with increasing β, first becoming flatter and then much more peaked in the centre, follows the trends already observed by Serizawa (1974) and Serizawa *et al.* (1975) for air–water flows but to a greater extent. The corresponding change in the shape of the turbulence intensity profile at first becoming flatter with increasing β is also similar to the results of Serizawa (1974) and Wang *et al.* (1986, 1987). However, the centreline peaking at high void fraction is opposite to the results for air–water flows.

The above results have illustrated the radial variation of various quantities with the volumetric quality as a parameter. It is also useful to examine the variation of some of these quantities with β, either at a fixed location, e.g. the centreline of the pipe, or values averaged over the cross-sectional area of the pipe. Assuming that $\epsilon(R) = \epsilon_{wall} = 0$ and, using the trapezoidal rule, the volume fraction may be integrated over the cross-sectional area of the pipe. The resulting area averaged values $\langle \epsilon \rangle$, are plotted against β in figure 7(a). Defining the average slip ratio H as the

ratio of the spatial average kerosene velocity to the spatial average water velocity, in a similar manner to Herringe & Davis (1974), its value can be determined from the relation

$$H = \frac{1/\langle \epsilon \rangle - 1}{1/\beta - 1}. \qquad [9]$$

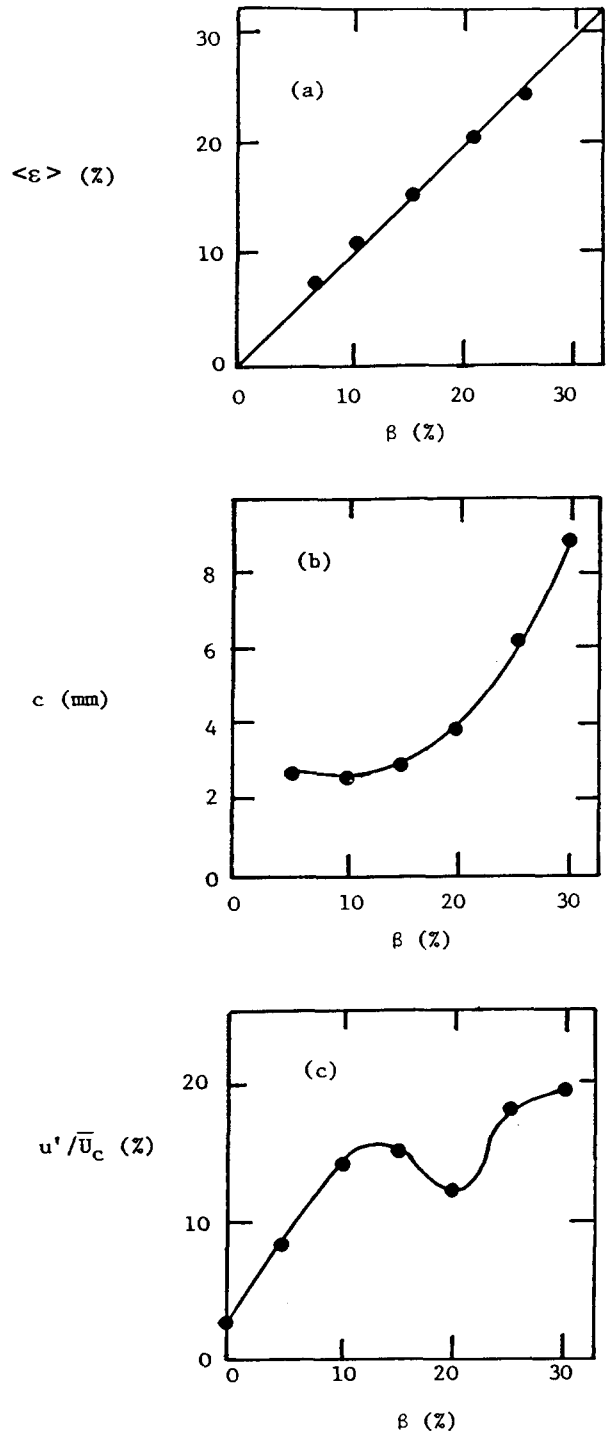

Figure 7. Variation with volumetric quality β of (a) area averaged volume fraction (b) centreline bubble cut cord length (c) centreline turbulence intensity.

The 45° line in figure 7 represents the situation in which $\langle \epsilon \rangle = \beta$, i.e. $H = 1$. Points above the line indicate that H is less than 1 and vice versa. It can be seen that at low volumetric quality, $\langle \epsilon \rangle$ is greater than β and the average slip ratio is less than 1, indicating that the average kerosene velocity is less than the average water velocity, even though, locally, the kerosene travels faster than the water due to buoyancy. This is because a large proportion of the kerosene travels in the outer regions of the tube close to the wall, where the local water velocity is relatively low. As β increases, the velocity profile initially becomes more uniform so that the above effect is not as pronounced. At still higher values of β the mean velocity profile becomes very peaked, but at this stage the bubbles in the central region are very large and travel at a much higher relative velocity than the small bubbles close to the wall. For this reason the average slip ratio becomes greater than unity as β increases.

Figure 7(b) shows the variation, at the pipe centreline, of the bubble cut cord length with the volumetric quality. As β increases the cord length remains approximately constant up to $\beta = 15\%$ before rising steeply. In a turbulent two-phase flow two major conflicting mechanisms interact to produce an equilibrium bubble size (Clift *et al.* 1978). Turbulence may cause the break-up of large bubbles while bubble collisions will in some cases lead to coalescence. The higher the turbulence intensity—and this increases with β—the more break up of bubbles takes place. However, a higher volume fraction also implies that the number of bubble collisions will increase and this provides a greater possibility of coalescence. Figure 7(b) suggests that up to a value of $\beta = 15\%$ the two mechanisms are in approximate equilibrium, but at higher β bubble coalescence dominates and large ellipsoidal/spherical cap bubbles are formed.

Figure 7(c) shows the variation in the turbulence intensity on the centreline with the volumetric quality. In a two-phase flow the turbulence intensity comprises two components, i.e. bubble generated turbulence and wall shear generated turbulent fluctuations. For the bubble generated turbulence, Sullivan *et al.* (1978) have related the turbulence energy production due to bubbles, to the total drag experienced by these bubbles as they rise through the continuous phase. For low volume fractions they give the relationship

$$u' = KU_\infty \sqrt{\langle \epsilon \rangle} \approx KU_\infty \sqrt{\beta} \qquad [10]$$

where K is a constant, so that the turbulence intensity varies approximately with the 1/2 power of the volumetric quality. Now, the rate of generation of wall shear turbulence kinetic energy is related to the value of the mean velocity gradient $(\partial \bar{U}/\partial r)$ in the near wall region. We can see from figure 5 that the velocity profile in the central region of the pipe first becomes more uniform with β, implying a steeper gradient near the wall and an increase in the shear generation of turbulence. These two mechanisms combine to give the initial step variation in u' with β shown in figure 7(c). When β is increased beyond 15% the mean velocity profile becomes centre peaked, leading to a reduction in the wall shear generated turbulence. This changeover is reflected as a local minimum at $\beta \approx 20\%$. Serizawa *et al.* (1975) have also found that the variation of turbulence intensity with β in air–water flow has a local minimum at low β before it increases with increasing β. Hino (1967) observed a similar phenomenon by introducing solid particles of small size into a liquid stream.

5.2. Bubbly flow, centreline measurements

More detailed measurements were made at the centreline of the pipe at $X/D = 17$. Results presented are in the form of the probability density function, $p(E)$, the autocorrelation function $R_{11}(\tau)$, and Taylor's one-dimensional energy spectrum $E_{11}(f)$.

Probability density function. Typical pdf results are shown in figure 8 for various values of β. All the pdf curves are seen to occupy a large proportion of the 0–10 Volt A/D range, and they display the characteristic bimodal shape first shown by Delhaye (1969). At $\beta = 5\%$, figure 8(a), the first modal peak, due to the dispersed phase, is of very small proportions and the plateau between the two peaks is also at a very low level. The tail of the pdf at the high voltage side extends to large values. This corresponds to the occasionally large overshoot seen in the signal as the probe passes through the rear of a bubble and into the continuous phase, as described in e.g. Bruun (1995). The local volume fraction ϵ was evaluated by the hot-film probe method as 6.2%. The volume fraction was also calculated by means of the method proposed by Delhaye (1969) in which the area under the pdf is divided into two parts, corresponding to the sensor being surrounded

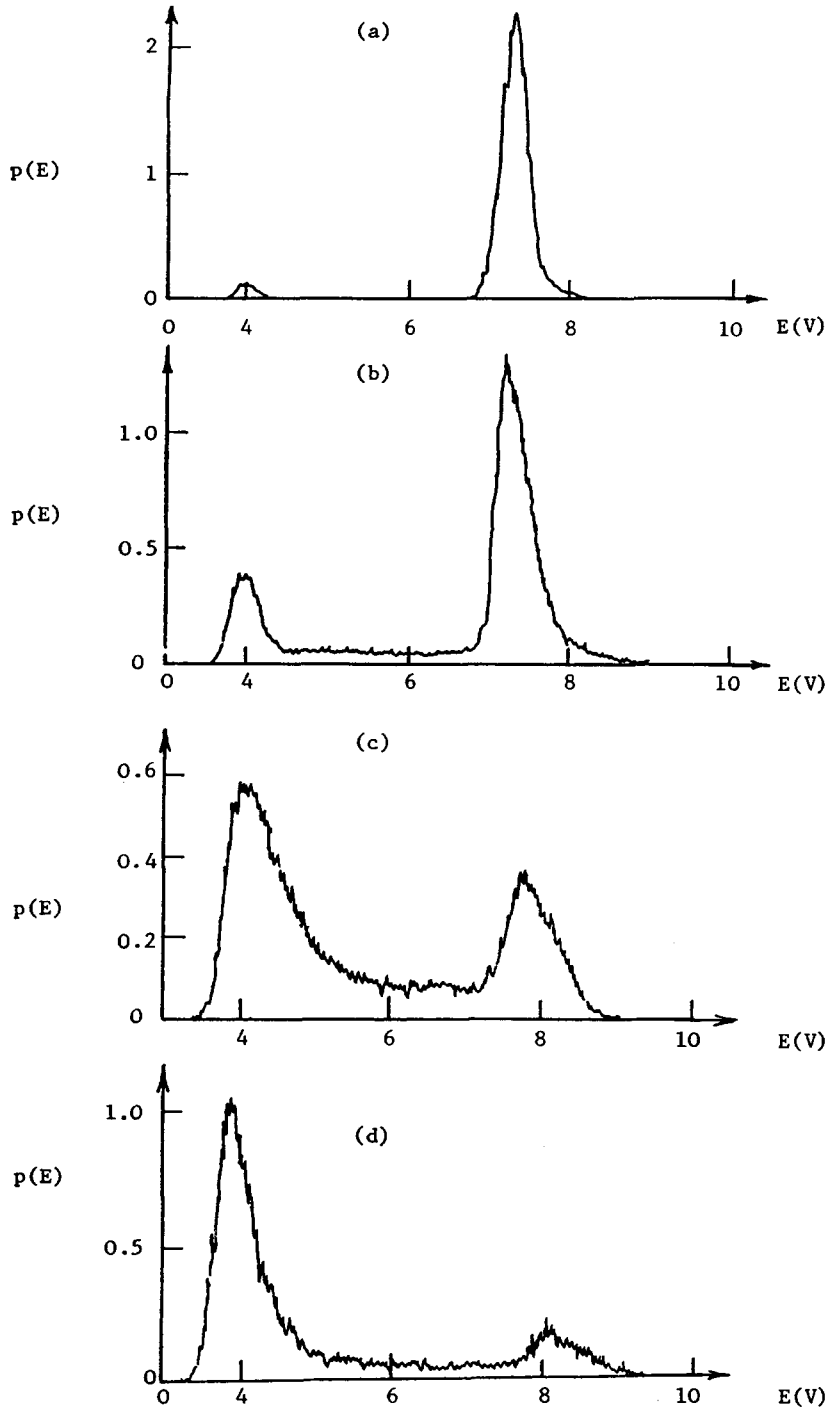

Figure 8. Pdf on pipe centre line. Bubble flow regime: (a) $\beta = 5\%$, (b) $\beta = 30\%$, (c) spherical cap bubble flow, $\beta = 62\%$, (d) churn flow, $\beta = 76\%$.

either by the continuous or the dispersed phase. This method yields a local volume fraction of 8.95%. The percentage error is very large but this is not unexpected since Delhaye proposed his method for the analysis of the signal from a conical probe and it is not directly applicable to cylindrical probes as discussed by Bruun & Farrar (1988). All the pdf curves obtained in the bubbly flow regime ($\beta < \sim 30\%$) were on the whole very similar, but some differences were noticeable. As expected, the first modal peak and the plateau region of the pdf increased in magnitude as β increased, as observed in the pdf curve corresponding to $\beta = 30\%$ (figure 8(b)). This obviously

resulted from the increased amount of the measurement time that the sensor spends in the dispersed phase, due to an increase in bubble numbers and bubble size, particularly for values of $\beta = 25\%$ and 30%.

The objective of the hot-film probe instrumentation part of this work (Farrar 1988; Bruun *et al.* 1995; Farrar *et al.* 1995) was to develop a hot-film anemometer based measuring system and technique for the investigation of two-phase bubbly kerosene in water flows. Conceptually, however, there is no reason why the technique should not be applicable to flows of higher kerosene volume fraction, and to evaluate this possibility additional tests were performed, on the pipe centreline, under conditions producing spherical cap bubble, churn and droplet (water dispersed) flow regimes. The tests were limited to the recording of the hot-film signal and the application of the volume fraction measuring software. The measured pdfs for the spherical cap bubble regime ($\beta = 62\%$) and for the churn flow regime ($\beta = 76\%$) are shown in figure 8(c) and (d).

For the spherical cap bubble flow an inspection of the unlinearised hot-film signal showed that there is a wide spread of bubble sizes with the occasional passage of a very large bubble. These are the large spherical cap bubbles which travel at high velocity along the centreline of the pipe. As described by Farrar & Bruun (1989) a water film may form between the prongs of the hot-film probe during the passage of a bubble. Breakage of this water film was observed in a number of cases to occur within bubbles and it was also noticed that there were several signals which must have been caused by the passage of two closely spaced bubbles. The current hot-film measurement method evaluated the volume fraction as $\epsilon = 73.3\%$. The plateau region of the pdf in figure 8(c) is not as flat or wide as for those obtained in bubbly flow, and the amplitude threshold selection method developed for the bubbly flow regime (see Farrar 1988) probably results in a threshold value which is slightly too large. A more suitable amplitude threshold for this flow would be a little lower.

Figure 8(d) shows an example of the pdf obtained in churn flow. The increase in volume fraction, which was evaluated as 87%, is obvious. The volumetric quality was 76%. An examination of the hot-film output signal showed that it did fit very well the description of churn flow in which neither phase is continuous and large blobs of kerosene-containing water droplets are interspersed with thin layers of water. For this type of flow measurements of turbulence in the kerosene phase would be more interesting. However, to obtain measurement of turbulence in the kerosene it would be necessary to use a hydrophobic coating on the surface of the sensor.

Autocorrelation function. Figure 9 contains the measured normalized autocorrelation function $R_{11}(\tau)$ at various volumetric qualities. In the water flow case, curve *a* ($\beta = 0\%$), $R_{11}(\tau)$ displays the conventional decay function shape due to the wall shear generated turbulence. At $\beta = 5\%$, curve *b*, the autocorrelation has been modified significantly, displaying a shape which is similar to that

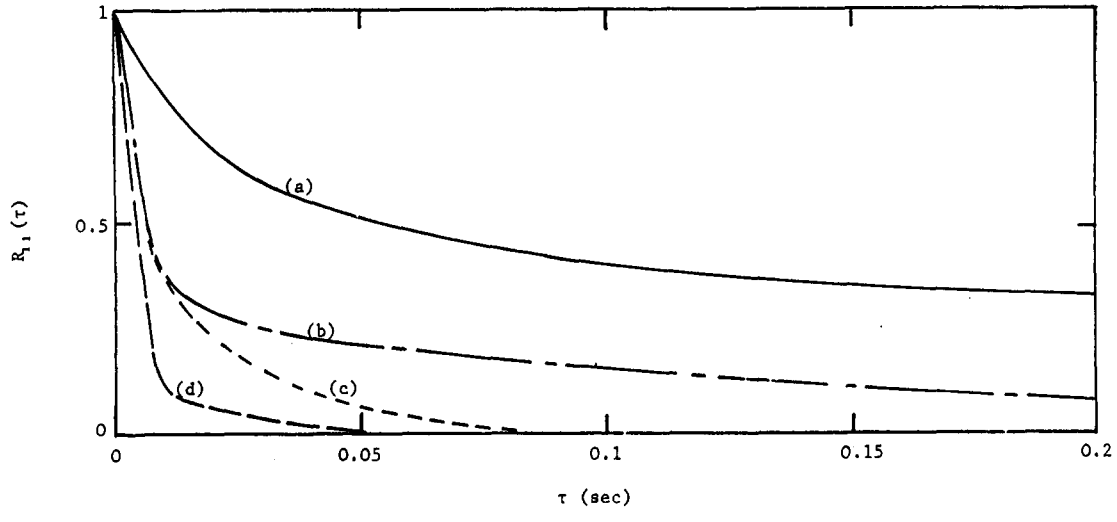

Figure 9. Auto correlation $R_{11}(\tau)$ at pipe centreline. (a) Single phase water flow. Kerosene–water flow: (b) $\beta = 5\%$, (c) $\beta = 15\%$, (d) $\beta = 30\%$.

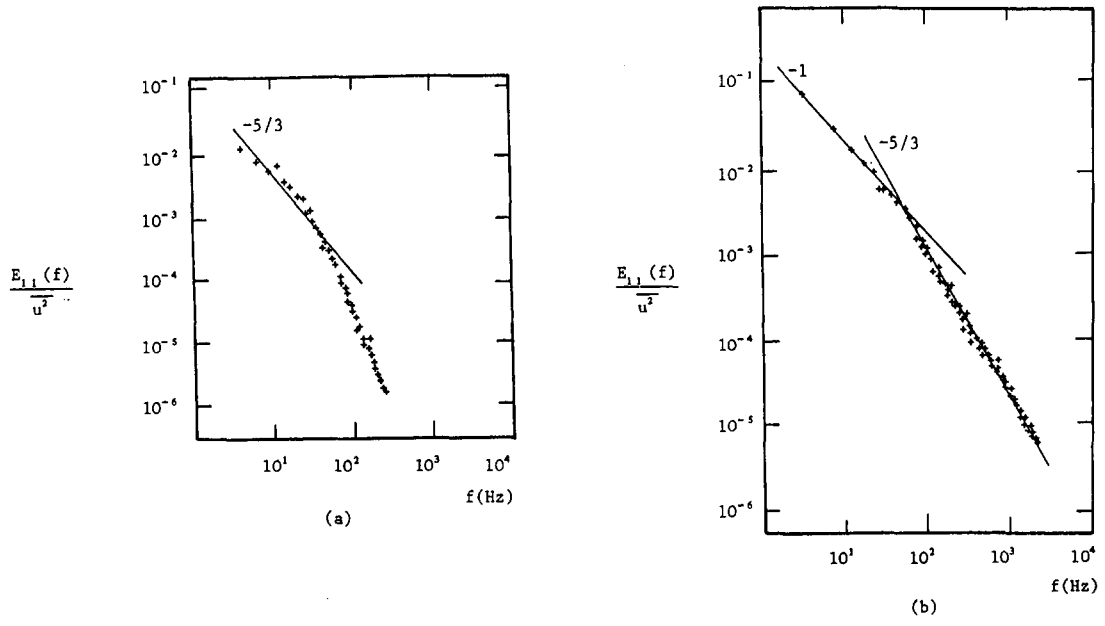

Figure 10. One-dimensional energy spectrum on pipe centreline (a) Single phase water flow, (b) Kerosene–water flow, $\beta = 20\%$.

obtained from the sum of two statistically independent stationary random processes of markedly different scales. Lumley & Panofsky (1964) and Townsend (1956) showed that such an autocorrelation curve will consist of an initial rapid decay followed by a much more gradual decay. In this case, the statistically independent processes are the two modes of turbulence generation in a two-phase flow, i.e. the small scale bubble generated turbulence and the larger scale wall shear generated turbulence. As the value of β was increased the initial region of the autocorrelation function retained the same shape but decayed to zero sooner, as illustrated by curve c ($\beta = 15\%$). At $\beta = 30\%$, curve d, the rapid decrease of $R_{11}(\tau)$ shows that the bubble generated turbulence now predominates.

Energy spectrum. The one-dimensional energy spectrum $E_{11}(f)$ was measured both for the single phase water flow and for the flow of the kerosene–water mixture. The spectrum for the water flow is shown in figure 10(a). On this figure the $-5/3$ slope is indicated and this clearly shows that no definite inertial subrange exists in this case due to the overlap of the ranges of scales associated with energy extraction and with energy dissipation. These findings agree well with the measurements of Laufer (1954) and Resch (1970).

In the bubbly flow regime it was found that all the one-dimensional energy spectra had similar shapes. The spectrum $E_{11}(f)$, shown in figure 10(b) for $\beta = 20\%$, is substantially different from the single-phase spectrum consisting very roughly of two straight lines of slope approximately -1 and $-5/3$ and displaying considerably more energy at higher frequencies. Consequently, to avoid aliasing, it was necessary to use a higher sampling rate of 5 kHz for these measurements.

In a stationary situation the spectral energy balance involves three mechanisms: viscous dissipation, spectral energy transfer and energy production, which at high wavelengths is caused by turbulent eddies formed in the bubbles' wakes.

Consequently, in the range of wavelengths in which energy is extracted from the flow by the bubble generated turbulence we would expect a considerable change in the shape of the spectrum when compared to that of single-phase flow. For an explanation of this, it is useful to introduce the schematisation of the spectral energy transfer given by Corrsin (1961) and shown in figure 11.

In a turbulent single phase pipe flow the length scale of the "eddies" which are responsible for extracting energy from the mean flow is of the order of D, the pipe diameter.

If the turbulent Reynolds number:

$$\mathrm{Re}_\lambda = \frac{u'\lambda}{\nu} \qquad [11]$$

where λ is Taylor's microscale and $u'(=\overline{(u^2)}^{1/2})$ is the rms fluctuating velocity, is large enough, then there is a range of frequencies between those at which the inflow and outflow of energy take place, in which there is a constant spectral energy transfer rate ϵ, as shown in figure 11(a). For the investigated single phase flow the value of Re_λ was evaluated as approximately 58, which is too low for a separate inertial subrange to exist.

In a two-phase flow, energy is also extracted from the flow by the bubble generated turbulence. This energy is extracted by "eddies" with a length scale of order d, the bubble diameter, which is an order of magnitude less than D in this investigation. Thus the spectral energy transfer in a two-phase may be as shown in figure 11(b), in which the total energy transfer rate is the sum of

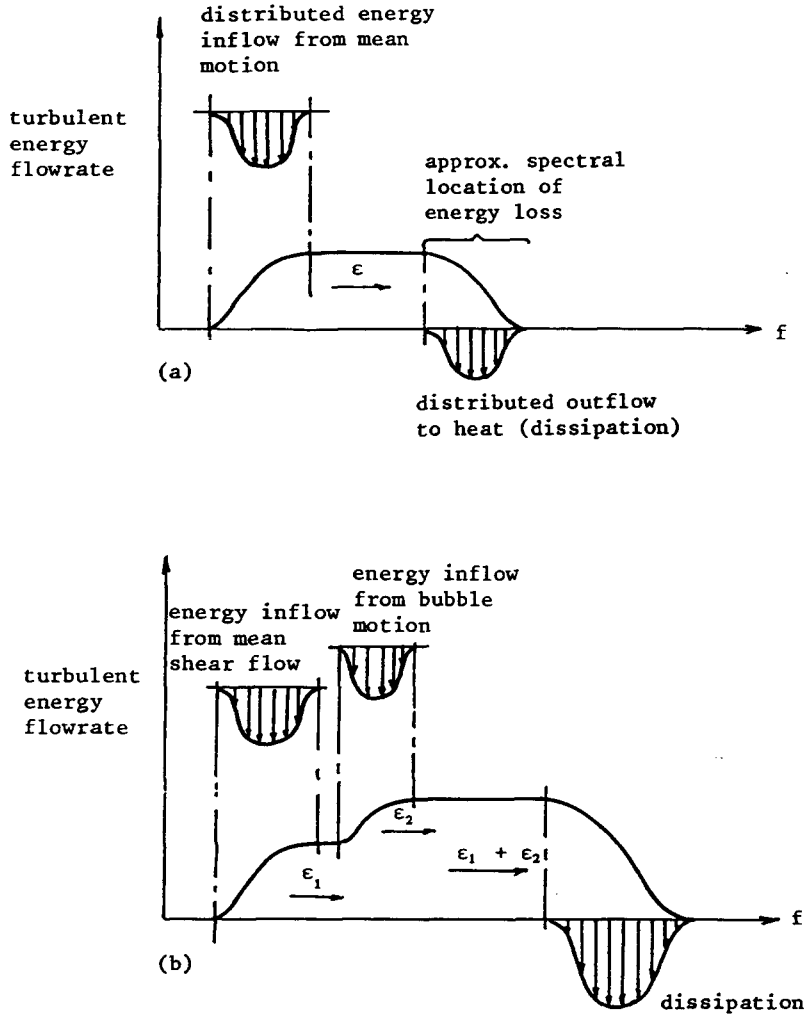

Figure 11. Schematic representation of spectral energy cascade. (a) Spectral energy cascade in single phase flow (after Corrsin 1961); (b) Spectral energy cascade in bubbly two-phase flow.

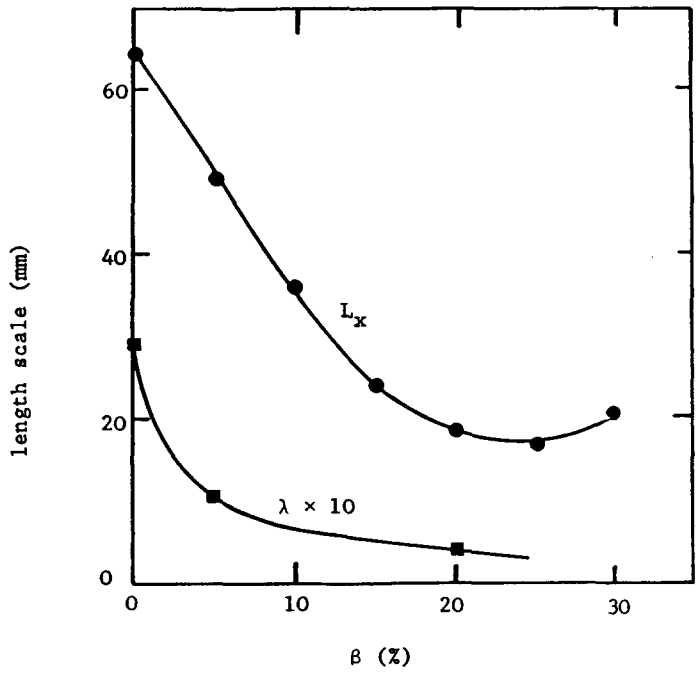

Figure 12. Variation in integral length scale and Taylor's microscale with volumetric quality β.

the two separate components ϵ_1 and ϵ_2 due, respectively, to the mean flow turbulence and to bubble generated turbulence. For the kerosene–water flow all the spectra obtained display a prominent inertial subrange in which the slope of the spectrum is $-5/3$. This implies that the energy dissipation is associated with much higher frequencies in two-phase flow. Indeed the turbulent Reynolds number increases to about 300 at $\beta = 30\%$, and this is well above the lower limit of 100 suggested by Reynolds (1974) for the existence of the inertial subrange.

Similar spectral measurements have also been carried out in air–water two-phase flow by, e.g. Lance & Bataille (1991). Their results for a uniform bubbly air-water flow with grid turbulence and low void fraction ($\epsilon < 5\%$) produced spectra with a typical slope of $-8/3$ instead of $-5/3$ as observed in our kerosene-water investigation. This indicates a different balance between the various terms in the spectral energy balance for the two types of flow.

Length-scales. Using Taylor's hypothesis, the longitudinal integral length scale, L_f, and Taylor's microscale, λ, were obtained from the autocorrelation function and the energy spectrum, respectively, as

$$L_f = \bar{U} I_u \qquad [12]$$

with

$$I_u = \int_0^\infty R_{11}(\tau)\, d\tau$$

and

$$\frac{1}{\lambda^2} = \frac{4\pi^2}{\bar{U}^2 u^2} \int_0^\infty f^2 E_{11}(f)\, df. \qquad [13]$$

The variation of both the integral length scale and Taylor's microscale with the volumetric quality is shown in figure 12. As expected, both fall as β increases. The integral length scale is reduced because the energy production becomes more associated with bubble generated turbulence with eddies of order D in size. The microscale falls because the increased turbulence energy must cascade to higher frequencies in order for viscosity to dissipate it.

6. CONCLUSIONS

This paper has described the application of a hot film anemometer flow measurement technique to the investigation of the structure of the vertical pipe flow of a water–kerosene mixture. Measurements were made for a range of operating conditions with the volumetric quality, β, varying from 5 to 30%. Radial profiles of the local continuous phase mean velocity and relative turbulence intensity, the volume fraction and mean bubble cut cord length have been made. The volume fraction profile is very uniform at low β but becomes wall peaked as β increases. For β less than 15%, the average bubble size is almost independent of β and r, but above 15% the bubble size at the pipe centreline increases significantly with β indicating that the flow regime is changing to spherical cap bubble flow. The increased mixing produced by the swarm of uniformly sized bubbles tends to flatten the velocity profile up to $\beta = 15\%$, but for $\beta > 15\%$ the larger bubbles at the centre of the pipe tend to drive the continuous phase at higher velocities and the velocity profile becomes very steep. The turbulence intensity at the pipe centreline contains contributions from turbulence generated by the mean shear flow and by the bubble wakes. The bubble generated turbulence increases monotonically with β, but the changes in mean velocity profile with β result in minimum mean shear generated turbulence at $\beta \approx 15$–20%. The resulting variation of turbulence intensity at the pipe centreline displays a local minimum region at $\beta \approx 20\%$.

The one-dimensional energy spectrum for the two-phase flow is basically composed of two power laws with exponents -1 at lower frequencies and $-5/3$ at higher frequencies. The integral length scale and the microscale decrease rapidly with increasing β signifying the increasing importance of bubble generated turbulence and its associated higher frequency fluctuations.

Acknowledgements—The authors would like to acknowledge the financial support and help given to them by Schlumberger Cambridge Research Ltd. The principal author also wishes to acknowledge the research studentship provided by the Science and Engineering Research Council.

REFERENCES

Beyerlein, S. W., Cossman, R. K. & Richter, H. J. 1985 Prediction of bubble concentration profiles in vertical turbulent two-phase flow. *Int. J. Multiphase Flow* **11,** 629–641.

Bruun, H. H. 1995 *Hot-wire Anemometry*. Oxford University Press, Oxford.

Bruun, H. H. & Farrar, B. 1988 Hot-film probe studies of kerosene/water and gas/liquid flows. In *Proceedings of the First World Conference on Experimental Heat Tranfer, Fluid Mechanics and Thermodynamics*, 4–9 September 1988, Dubrovnik, Yugoslavia (Edited by R. K. Shah, E. N. Ganic & K. T. Yan), pp. 371–379. Elsevier, New York.

Bruun, H. H. & Samways, A. L. 1995 Hot-film measurements techniques in two-phase flows. In *International Symposium on Measuring Techniques for Multiphase Flows*. Nanjing, China, April 10–13.

Bruun, H. H., Samways, A. L. & Ali, J. 1995 A hot-film study of oil/water flow in a vertical pipe. In *Second International Conference on Multi-phase Flow*. Kyoto, Japan, 3–7 April.

Clift, R., Grace, J. R. & Weber, M. E. 1978 *Bubbles, Drops and Particles*. Academic Press, New York.

Corrsin, S. 1961 Turbulent flow. *American Scientist* **49,** 300–325.

Delhaye, J. M. 1969 Hot-film anemometry in two phase flow. In *Proc. 11th Nat. ASME/AIChE Heat Transfer Conf. on Two-phase Flow Instrumentation*, Minneapolis, Minnesota, pp. 58–69.

Drew, D. A. & Lahey, R. T. 1987 The virtual mass and lift force on a sphere in rotating and straining inviscid flow. *Int. J. Multiphase Flow* **13,** 113–121.

Farrar, B. 1988 Hot-film anemometry in dispersed oil–water flows. Ph.D. Thesis, Department of Mechanical and Manufacturing Engineering. Bradford University.

Farrar, B. & Bruun, H. H. 1988 Hot-film probe measurements in kerosene–water flows. In *Second UK National Conference on Heat Transfer*, University of Strathclyde, UK, pp. 1269–1279, 14–16 September.

Farrar, B. & Bruun, H. H. 1989 Interaction effects between a cylindrical hot-film anemometer probe and bubbles in air–water and oil/water flows. *J. Phys. E. Sci. Instr.* **22,** 119–123.

Farrar, B., Samways, A. L., Ali J. & Bruun H. H. 1995 A computer based hot-film technique for two-phase flow measurements. *Meas. Sci. Techn.* **6,** 1528–1537.

Herringe, R. A. & Davis, M. R. 1976 Structural development of gas–liquid mixture flows. *J. Fluid Mech.* **73,** 97–123.

Hino, M. 1967 Micro-structure of solid–liquid two-phase flow. In *Proc. Symp. on Multi-phase Mixtures*, prepared by Sci. Council of Japan, pp. 21–30.

Jones, O. C. & Zuber, N. 1978 Use of a cylindrical hot-film anemometer for measurement of two-phase void and volume flux profiles in a narrow rectangular channel. *AICHE Symp Ser.* **74,** 191–204.

Kataoka, I. & Serizawa, A. 1990 Interfacial area concentration in bubbly flow. *Nucl. Enging Des.* **120,** 163–180.

Knitmesh 1982 Knitmesh liquid/liquid separation catalogue, No. LL6, Knitmesh Limited, Sanderstead Station Approach, South Croydon, CR2 OYY.

Lahey, R. T. 1990 The analysis of phase separation and phase distribution phenomena using two-fluid models. *Nucl. Engng Des.* **122,** 17–40.

Lance, M. & Bataille, J. 1991 Turbulence in the liquid phase of a uniform bubbly air–water flow. *J. Fluid Mech.* **222,** 95–118.

Laufer, J. 1954 The structure of turbulence in fully developed pipe flow. NACA Rep. 1174.

Liu, T. J. & Bankoff, S. G. 1993 Structure of air–water bubble flow in a vertical pipe—1. Liquid mean velocity and turbulence measurements. *Int. J. Heat and Mass Transf.* **36,** 1049–1060.

Lumley, J. L. & Panofsky, H. A. 1964 *The Structure of Atmospheric Turbulence.* Interscience Monographs and Texts in Physics and Astronomy. John Wiley and Sons, New York.

Michiyoshi, I & Serizawa, A. 1986 Turbulence in two-phase bubbly flow. *Nucl. Engng Des.* **95,** 253–267.

Moursali, E., Marie, J. L. & Bataille, J. 1995 An upward turbulent bubbly boundary layer along a vertical flat plate. *Int. J. Multiphase Flow* **21,** 107–117.

Reynolds, A. J. 1974 *Turbulent Flows in Engineering.* Wiley-Interscience, John Wiley and Sons, New York.

Resch, F. J. 1970 Hot-film turbulence measurements in water flow. In *Proc. ASCE, J. Hyd. Div.*, Vol. 96, No. HY3, pp. 787–800.

Samways, A. L., Ali, J., Al-Deen, M. F. N. & Bruun, H. H. 1994 The calibration and measurements with cylindrical hot-film probes in water flows. *Meas. Sci. Technol.* **5,** 1551–1559.

Sato, Y. & Sekoguchi, K. 1975 Liquid velocity distribution in two-phase bubble flow. *Int. J. Multiphase Flow* **2,** 79–95.

Serizawa, A. 1974 Fluid dynamic characteristics of two-phase flow. Ph.D. Thesis, Institute of Atomic Energy, Kyoto University, Japan.

Serizawa, A. & Kataoka, I. 1987 Phase distribution. In *ICHMT Int. Seminar on Transient Phenomena in Multiphase Flow*, pp. 179, Dubrovnik, Yugoslavia.

Serizawa, A. & Kataoka, I. 1992 *Dispersed flow.* In *Proc. 3 Int. Workshop on Two-phase Flow Fundamentals*, June 15–19, London, UK.

Serizawa, A., Kataoka, I. & Michiyoshi, I. 1975 Turbulence structure of air–water bubbly flow, parts I–III. *Int. J. Multiphase Flow* **2,** 221–259.

Souhar, M. 1989 Some turbulence quantities and energy spectra in wall region in bubble flow. *Phys. Fluids* **A1,** 1558–1565.

Sullivan, J. P., Houze, R. N., Buenger, D. E. & Theofanous, T. G. 1978 Turbulence in two-phase flows In *2nd Annual CSNI Specialist Meeting of Transient Two-phase Flow*, Paris, France, June 12–14, 1978, pp. 583–608.

Theofanous, T. G. & Sullivan, J. 1982 Turbulence in two-phase dispersed flows. *J. Fluid Mech.* **116,** 343–362.

Tomiyama, A., Sou, A., Zun, I., Kanami, N. & Sakagushi, T. 1995 Effect of Eotvos number and dimensional liquid volumetric flux on lateral motion of a bubble in a laminar duct flow. In *Proc. 2nd Int. Conf. on Multiphase Flow*, pp. PD1 11–18, 3–7 April, Kyoto, Japan.

Townsend, A. A. 1956 *The Structure of Turbulent Shear Flow.* Cambridge University Press, Cambridge.

Wang, S. K., Lee, S. J., Jones, O. C. & Lahey, R. T. 1986 Three-dimensional conical probe measurements in turbulent air/water two-phase pipe flow. T.S.I. Flow Lines, Fall 1986.

Wang, S. K., Lee, S. J., Jones, O. C. & Lahey, R. T. 1987 3-D turbulent structure and phase distribution measurements in bubbly two-phase flow. *Int. J. Multiphase Flow* **13,** 327–343.

Zun, I. 1980 The transverse migration of bubbles influenced by walls in vertical bubbly flow. *Int. J. Multiphase Flow* **6,** 583–588.

Zun, I. 1988 Transition from wall void peaking to core void peaking in turbulent bubbly flow. In *Proc. Transient Phenomena in Multiphase Flow*—ICHMT Int. Seminar, Dubrovnik, pp. 225–245.

Zun, I., Richter, H. J. & Wallis, G. B. 1975 The transverse migration of bubbles in vertical two-phase flow. Dartmore College. Thayer School of Engineering. Hanover, NH.